BRIEF REPORT

Rethinking the statistical parameters of a large-scale reionization model

H. Baraer[a,1]
Supervised by : Prof. A. Liu[a,2]

[a]McGill University 845 Sherbrooke Street W Montréal, Quebec H3A 0G4

This manuscript was compiled on December 11, 2022

The study of the reionization history of neutral hydrogen composing the intergalactic medium ($20 \gtrsim z \gtrsim 6$) plays a crucial role in our understanding of the universe's structure. Prior to Battaglia et al. in 2013 (1), only short-scale models ($\lesssim Mpc\, h^{-1})^3$ included radiative transfer simulations and hydrodynamics. The Battaglia model can construct reionization redshift fields from any density field through a linear bias term accounting for radiative transfer and hydrodynamics, even at large scales ($\gtrsim Gpc\, h^{-1})^3$. However, the lack of physical understanding of the three free parameters forming this linear bias makes the model difficult to use. This project aims to link these free parameters to a semi-numerical model that uses a more direct approach based on parameters with physical meaning, called 21cmFAST. The presented algorithm computes the linear bias factor from 21cmFAST data and fits it using bayesian inference and Markov Chain Monte Carlo. Results show that the algorithm successfully links 21cmFAST with the linear bias and that the simple, functional form of the bias proposed by Battaglia et al. fits the data well. Future steps involve quantitative analysis of the effect of cosmological parameters fluctuations on the posterior distributions of the free parameters.

Cosmology | Epoch of Reionization | Numerical Simulations | Markov Chain Monte Carlo | Model Comparison

Introduction

Following the Big Bang, the universe was composed of a hot and dense "soup" of fundamental particles. The universe cooled and expanded for about 380 000 years. On the redshift scale used in cosmology to measure time, it corresponds to a redshift: z ≈ 1100. This cooling and expansion continued until the universe became cool enough to allow electrons and protons to combine, forming the first neutral hydrogen atoms(2). This process is called recombination, even if it is the first time the proton-electron combination has happened. This naming contradiction is due to the process being named prior to the understanding of the Big Bang (3). Following recombination, observations are limited as the absorbing effect of the neutral hydrogen composing the universe made it opaque on shorter wavelengths. This epoch known as the dark ages lasted about 250 million years, from redshifts $1100 \gtrsim z \gtrsim 20$. During that period, regions of the universe with higher gas density slowly collapsed under gravity and formed the first stars.

As the first stars ignited, their photons ionized the neutral hydrogen of their surroundings. These first bubbles of ionized gas started a process of ≈ 750 million years, in which almost all of the neutral hydrogen in between stars, known as the intergalactic medium (IGM), reionized. This epoch of transition of the IGM is called the Epoch of Reionization (EoR) and occurred from redshifts $20 \gtrsim z \gtrsim 6$ (4).

The reionization occurred in an inhomogeneous process, meaning different parts of the IGM reionized at different redshifts. Understanding the reionization history of the IGM in the EoR is crucial in our understanding of the first stars' formation and our understanding of the current structure of our universe (5). This reionization history can be modeled through the redshift of reionization field, a three-dimensional field of our universe showing the redshift at which each region of the IGM reionized. As neutral hydrogen is observable, precise theoretical models of the redshift of the reionization field are necessary to interpret observations. Moreover, these models must be on large scales ($\gtrsim Gpc$) since a representative sample of the stars, the ionizing source, is necessary for a precise model.

Prior to a model proposed by Battaglia et al. in 2013 (1), direct simulations of the evolution of the reionization field in large volumes $(\gtrsim Gpc\, h^{-1})^3$ were not attainable. There exist two types of models for the redshift of reionization. Firstly, short $(\lesssim Mpc\, h^{-1})^3$ scale models exists (6) (7), that use various gas physics and hydrodynamic implementations to capture the essential physics of reionization with a high resolution. However, reaching a resolution small enough to represent the reionization physics in the required larger scales is impossible given current computational powers. On the other side, there exist semi-analytical models based on simpler relations (8) (9). Although these semi-analytical models represent the basic properties of the EoR, they omit important radiative transfer and hydrodynamic properties, hence lacking in precision.

The Battaglia model (1) represents a hybrid solution: a semi-analytical model with a statistical component representing hydrodynamic and radiative transfer simulations. This solution allows direct simulations of the redshift of reionization field in large volumes. To do so, it quantifies a relation between the density field and the redshift of reionization field on small scales. A density field is a three-dimensional box representing the inhomogeneous density regions in our universe, and precise high-resolution field simulations are less computationally heavy. The model links a particle-particle-particle-mesh (P^3M) simulation of 2048^3 dark-matter particles, 2048 gas

The following people are involved

[1]The main author of this report is Hugo Baraer. E-mail: hugo.baraer@mail.Mcgill.ca

[2]This project is done under the supervision of Prof. Adrian Liu. E-mail: Adrian.liu2@mcgill.ca

cells and 17 billion adaptive rays to a short-scale reionization model. This reionization model combines a radiative transfer algorithm and a cosmological hydrodynamic code. Both fields are then converted into fluctuation fields. Fluctuation fields are computed with the average of their fields, showing the relative differences from the mean rather than the values themselves. As an example, for the density field, its fluctuation field would show how much each regions of our universe differs from its mean density, rather than the density of the region itself. They are easier to deal with, as they are unitless, making correlations in between fields more easily quantifiable. The fluctuation field for the density field, called the over-density field ($\delta(m)$), is defined as follow :

$$\delta_{\rm m}(\mathbf{x}) = \frac{\rho(\mathbf{x}) - \bar{\rho}}{\bar{\rho}}, \quad [1]$$

where $\bar{\rho}$ is the mean density of the universe. The fluctuation field for the redshift of reionization field, called the over-redshift of reionization field ($\delta(z)$), is defined as follow:

$$\delta_z(\mathbf{x}) = \frac{[1 + z_{\rm RE}(\mathbf{x})] - [1 + \bar{z}]}{1 + \bar{z}}, \quad [2]$$

where $\bar{z}$ is the mean redshift of reionization. The Fourrier transform of both fluctuation field is then taken, such that $\delta_z(\mathbf{x}) \rightarrow \tilde{\delta}_z(\mathbf{k})$ and $\delta_m(\mathbf{x}) \rightarrow \tilde{\delta}_m(\mathbf{k})$. A linear bias factor is computed, such that it satisfies the following equation:

$$\tilde{\delta}_{\rm z}(k) = b_{mz}(k)\tilde{\delta}_{\rm m}(k). \quad [3]$$

To compute the factor, their correlation is quantified using two-point statistics in Fourier space. I.e., the model compute the power spectrum of each field. Power spectrums are the equivalent of correlation functions in momentum space, and can be defined as :

$$\left\langle \left| \widetilde{\delta_m}(\mathbf{k}) \right|^2 \right\rangle \propto P_{mm}(\mathbf{k}), \quad [4]$$

and

$$\left\langle \left| \widetilde{\delta}_z(\mathbf{k}) \right|^2 \right\rangle \propto P_{zz}(\mathbf{k}), \quad [5]$$

,

where the brackets $\langle\rangle$ denotes an ensemble average. The linear bias factor b_{mz} is defined as being the square root of the power spectrum ration :

$$b_{\rm mz}(k) = \sqrt{\frac{P_{zz}(k)}{P_{\rm mm}(k)}}. \quad [6]$$

This factor can be fitted by a thee-parameter function, and its simple functional form can be written as:

$$b_{\rm mz}(k) = \frac{b_{\rm o}}{(1 + k/k_{\rm o})^{\alpha}}, \quad [7]$$

where α, b_0 and k_0 are free parameters. Thanks to these parameters, the model can successfully simulate precise reionization redshift fields on a larger scale. However, one problem pointed out by the authors of this model is the lack of physical understanding of the three free parameters of equation 7 (α, b_0 and k_0). A physical interpretation of these parameters would allow an understanding of the physics behind the correlation between density and the reionization redshift and would facilitate the use of the model.

Another model proposed by Messinger et al. in 2011 (10), named 21cmFAST, proposes a semi-numerical model that uses a more direct approach based on parameters with physical meaning. It computes the redshift of reionization field and the density field independently. It uses a halo finder to search for hydrogen bubbles and consider a pixel of the redshift of reionization field fully ionized where the collapse fraction meets a set efficiency parameter. 21cmFAST is a C algorithm with a Python envelope. On the downside, 21cmFAST is computationaly slower than the Battaglia et al. model, and doesn't include hydrodynamic simulations. It is possible to fit Battaglia et al.'s linear bias to the 21cmFAST model and vary the physical parameters, like the above-described ionization efficiency parameter. Doing so would link the statistical free parameters of the linear bias in Battaglia et al. to the physical ones used in 21cmFAST. Therefore, there is a need for an algorithm linking the linear bias factor of Battaglia et al. with the 21cmFAST model.

This project aims to construct an algorithm linking the free parameters of the linear bias in Battaglia et al. to the redshift of reionization field and the density field generated from 21cmFAST. This project also aims to verify the validity of the linear bias's functional form (equation 7) when applied to models containing no hydrodynamic simulations, like 21cmFAST. This report presents the work done during the fall semester in the context of PHYS 449: a major research project.

Methods

Here is presented the series of steps used to link the linear bias factor of Battaglia et al. with the 21cmFAST model. Since the 21cmFAST algorithm generates density fields and reionization redshift plots independently, this algorithm follows the same steps that the Battaglia model uses to calibrate their linear bias factor, but this time with models not including radiative transfer and hydrodynamics simulation. A schematic of the steps taken by the algorithm is presented in Figure 1.

In Cosmology, some parameters do not have a consensus value and can vary in the literature. These parameters includes the Hubble parameter $h = H_0/100 kms^{-1}Mpc^{-1}$, the density proportion of matter Ω_m, and the density proportion of dark energy Ω_Λ. In this work, these values are set to : $\Omega_{\rm m} = 0.27, \Omega_\Lambda = 0.73, h = 0.7$

The algorithm is Python-based and interacts directly with the 21cmFAST model. It is composed of a driver file, *standard_driver.py*, interacting with 4 different modules: *z_re_field.py*, *Gaussian_testing.py*, *FFT.py* and *statistical_analysis*. A testing script, *test_modules*, is also available to test the different built-in function. The following subsections present the different steps and the role of each module.

Computing the fluctuation fields

The first part of this project is to compute the fluctuation fields: the over-density field and the over-redshift of reionization field. This is done with the *z_re_field.py* module. The generated three-dimensional fields represents a cubic universe of dimensions $100\frac{Mpc}{h}$ x $100\frac{Mpc}{h}$ x $100\frac{Mpc}{h}$. The spatial resolution is $1\frac{Mpc}{h}$, meaning each voxels (a voxel is

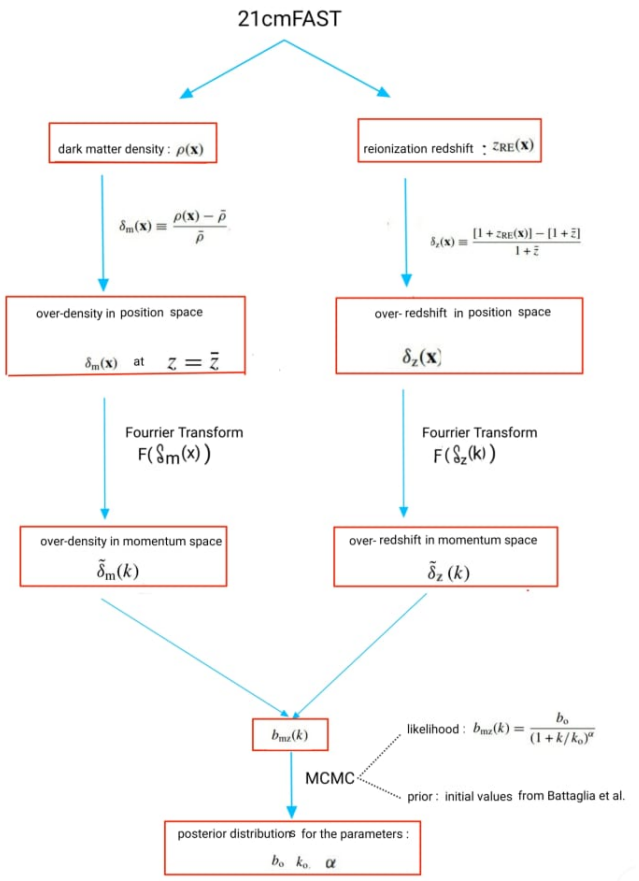

Fig. 1. Schematics of the process used in this project. The red boxes represent a three-dimensional field. The blue arrow with its corresponding equation represents the transformation done to the field to bring it to the next step. The MCMC stands for Markov Chain Monte Carlo

a three-dimensional pixel) represents $1\frac{Mpc}{h}^3$ of our universe. The h^{-1} factor makes it independent of the Hubble parameter. As an example, 1 Mpc/h corresponds to 1.43 Mpc when $h = 0.7$.The dimensions chosen are the same as the one used in the Battaglia et al. model.

Firstly, for the redshift of reionization field, 21cmFAST does not have the option to compute it directly and only computes the ionization field at a given redshift $\chi(x, z)$. Therefore the redshift of reionization field is computed by parsing through the ionization field at different redshifts.

Secondly, the coeval cube function of the 21cmFAST model is used to generate a density field. As the density field is redshift dependent, it is computed at the mean redshift of reionization ($\bar{z} = 7.22$). This mean corresponds to the computed mean value of the redshift of reionization field.

The fields are then converted into their fluctuation fields, the over-density and the over-redshift of reionization through equations 1 and 2 respectively.

Fast Fourier transforms

Using the module *FFT.py*, and NumPy's module *FFT*, standing for fast Fourier transform, a Fourier transform is performed on the fluctuation fields with NumPy's extension *fft*. Numpy's FFT algorithm makes assumptions about the origin placement that can alter results. To counter that effect, the module *Gaussian_testing.py* simulates a perfect three-dimensional Gaussian in a three-dimensional field with the same dimensions as the previously computed fields. Knowing that a Gaussian field in momentum space is also a Gaussian, a shift in the origin placement of the Gaussian field is applied until the field in momentum space returns that wanted Gaussian. These same changes are then applied when taking the Fourier transform of the fluctuation fields.

The linear bias

To compute the linear bias, the same logic used by the Battaglia model in section is applied. Following equations, 4 and 5 the magnitude of both the over-density and the over-redshift of reionization in momentum are taken and squared. Taking the average of these fields consists of converting the three-dimensional field into a one-dimensional array where the independent variable is the frequency k which is the inverse of the voxel's distance from the center of the field. To do so, the fields are converted in spherical coordinates so that $\delta(k_x, k_y, k_z) \rightarrow \delta(k, \theta, \phi)$ where $k = \sqrt{k_x^2 + k_y^2 + k_z^2}$. The fields are then averaged over phi and theta. I.e., the field is separated into spherical shells varying by a defined radius, and each of the shells is averaged to one value. This averaging is done in the module *statistical_analysis.py*.

Fitting 21cmFAST data to the 3 parameter function

With the the linear bias $b_{mz}(k)$ computed, the module *statistical_analysis.py* fits the data to the three-parameter function described by equation 7. To do so, it performs Bayesian inference with a Markov Chain Monte Carlo (MCMC). Bayesian inference infers probability distributions, giving the best-fit parameters a continuous distribution. Markov Chain Monte Carlo (MCMC) is a class of methods for sampling a probability density function using a Markov chain whose equilibrium distribution is the desired distribution (11). MCMC is a sampling algorithm that executes a biased random walk among the possible best-fit values, spending more time on high probability regions and inferring parameter distribution. Combining MCMC with Bayesian inference allows exploring parameter space and finding the posterior high probability region.

Errors and uncertainties

Errors and uncertainties evaluation is a significant part of this project. Since fitting with MCMC depends on errors, It is crucial to have appropriate errors bars for the linear bias. Since this work is based on theoretical models approximating reality, the extend of the systematic uncertainty is almost impossible to define. However, this project performs an averaging when computing the power spectrum. Assuming a Gaussian distribution in each of the shells, the standard error SE of the sampling distributions P_{mm} and P_{zz}, can be expressed as:

$$SE = \frac{\sigma}{\sqrt{N}}, \qquad [8]$$

where N is the number of voxels per shell, and σ is the

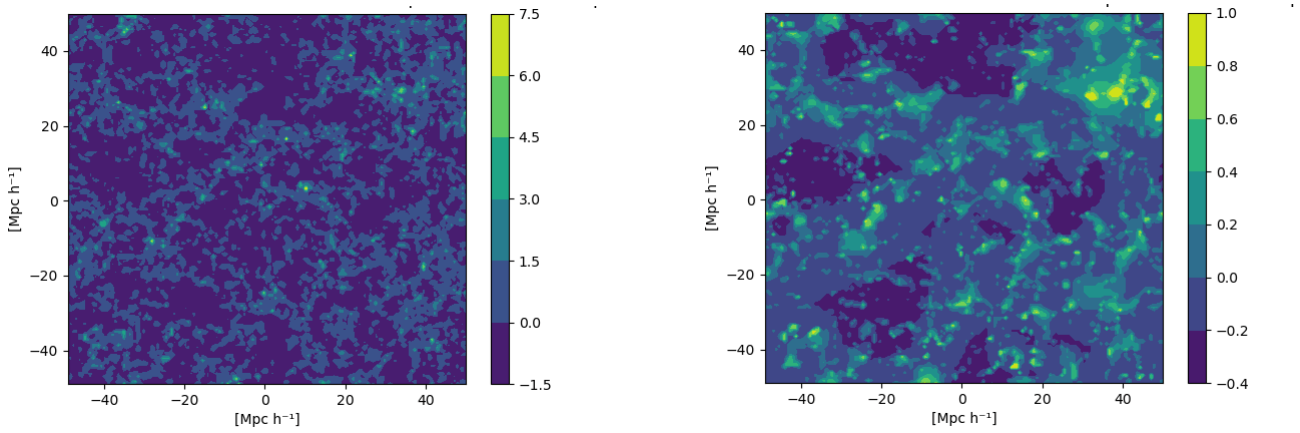

(a) Slice of the over-density $\delta_m(x)$ field at $\bar{z} = 7.22$

(b) Slice of the over-redshift of reionization field $\delta_z(x)$

Fig. 2. Comparison between the over-density at the mean redshift of reionization: $\bar{z} = 7.22$, and the over-redshift of reionization. The colour scale of the left panel illustrates the deviation of matter density from the mean, with denser region leaning toward brighter tones. The colour scale in the right panel illustrates the deviation from the mean redshift at which the hydrogen of the IGM reionized, with older, higher redshift reionization leading toward brighter tones. Both plots represent two-dimensional slices of three-dimensional fields, sliced at the same place in the third dimension. Both plotted windows are $100\frac{Mpc}{h}$ by $100\frac{Mpc}{h}$, with a pixel resolution of $(1\frac{Mpc}{h})^2$

standard deviation stated as follow :

$$\sigma = \sqrt{\frac{\sum (x_i - \mu)^2}{N}} \quad [9]$$

In the above equation, μ is the mean value of the shell, and x_i is the value of the computed voxel. When computing the linear bias with equation 6, the standard error of both power spectrums propagates. The error in the linear bias factor σ_b can therefore be computed following error propagation rules:

$$\sigma_{bmz} = b_{mz}\sqrt{\left(\frac{1\sigma_{\delta m}}{2\delta_m}\right)^2 + \left(\frac{1\sigma_{\delta z}}{2\delta_z}\right)^2} \quad [10]$$

Results

In this section, results from the different steps of the algorithm are presented.

The fluctuation fields

Figure 2 presents the over-redshift of reionization and the over-density in position space. The cubes are sliced to produce a two-dimensional colour plot, since the fields are three-dimensional. The slice occurs at the middle of the cube so that the slice is centered on the z-axis. Both fields have dimensions of $(100\frac{Mpc}{h})^3$. The presented slices are of thickness $1\frac{Mpc}{h}$, with a pixel resolution of $(1\frac{Mpc}{h})^2$. The slices exhibit similar regions of low and high fluctuations. For example, the top-right corner of the over-density plot shows high-density zones, while the same top-right corner in the over-redshift of reionization shows zones of the reionization that occurred at higher redshift. This symmetry is visible throughout the entire slices. Even tho they were computed independently with 21cmFAST, the fields are visually correlated. This gives confidence in the process of computation of the redshift of reionization. Furthermore, scaling for over-redshift of reionization is in concordance with previous literature models (12).

The Fourier transformed fields

Figure 3 presents the magnitude square of the fluctuation fields in momentum space. The cubes are sliced to produce a two-dimensional colour plot as the fields are three-dimensional. The slice occurs at the middle of the cube so that the slice is centered on the k_z axis. The plotted slice are zoomed versions of the computed fields slice, as the field in their computed size contained a large amount of blank space. Dimensions of the computed field are $1\frac{h}{Mpc}$ x $1\frac{h}{Mpc}$ x $1\frac{h}{Mpc}$, while Figure 3 presents a window of $0.5\frac{h}{Mpc}$ x $0.5\frac{h}{Mpc}$. Both fields show a high concentration towards the center, low k values, and an exponential decay when leaning towards higher k values. A rotational symmetry around the origin is visible in both fields. As symmetry is a property of Fourier transform, Figure 3 suggests properly computed Fourier transforms. Both fields present a similar scale, with $|\tilde{\delta_m}(k)|^2$ than $|\tilde{\delta_m}(k)|^2$ decaying slower in the $|0.1| < k < |0.2|$ range.

The linear bias

Figure 4 presents the computed linear bias linking the over-redshift of reionization to the over-density in momentum space, following equation 4, 5 and 6. A clear and smooth exponential decay is visible. Errors bars also decrease exponentially. As the value of k for the center shells of the fluctuation fields in momentum space is much higher, it is logical that the error bars also would. The last data point of Figure 4 appears to be skewed. One hypothesis for this is the origin placement in NumPy's *FFT* algorithm. Since the origin is not necessarily at the center, the furthest k might only have values of one of the sides, making it biased as it does not consider the rotational symmetry. The shape and behaviour of this computed bias factor are in agreement with the one in Battaglia et al.

Fitting

Testing the algorithm showed that fitting for the pa-

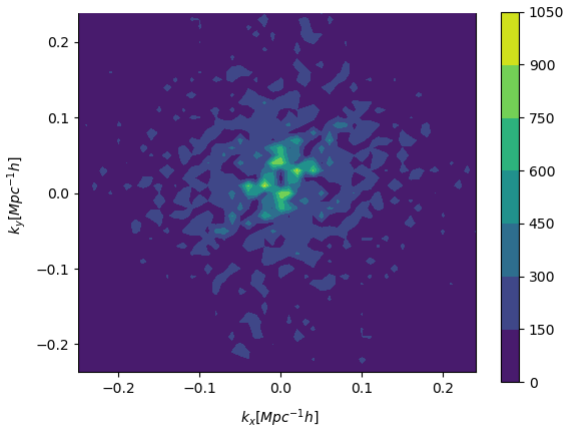

(a) Slice of the magnitude square of the Fourier transform of the over-density field at $\bar{z} = 7.22$ $|\tilde{\delta_m}(k))|^2$.

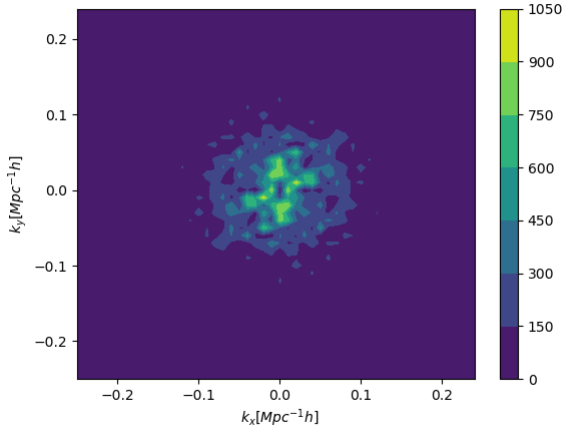

(b) Slice of the magnitude square of the Fourier transform of the over-redshift of reionization field $|\tilde{\delta_z}(k))|^2$.

Fig. 3. Comparison between the magnitude square of the over-density at the mean redshift of reionization $\bar{z} = 7.22$, and the over-redshift of reionization, both in momentum space. The colour scale of the panels illustrates the magnitude of the frequency, with more prominent frequencies leaning toward brighter tones. Both plots represent two-dimensional slices of three-dimensional fields, sliced at the same place in the third dimension. Both plotted windows are $0.5\frac{h}{Mpc}$ by $0.5\frac{h}{Mpc}$, with a pixel resolution of $0.01\frac{h}{Mpc}$

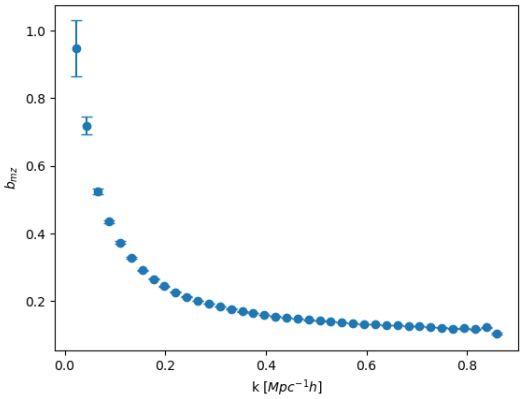

Fig. 4. The linear bias factor as a function of the wavenumber k. Each data point represents the ratio of the averaged over-redshift of reionization field and the over-density field, with error bars corresponding to the standard errors of these averages. b_{mz} decreases rapidly on scale below $0.1\frac{h}{Mpc}$.

rameter b_0 degenerates with k_0 and α. In Battaglia et al., this parameter is not fit for, as b_0 applies on scales larger than the field fitted on. As the same field dimensions are used in this project, b_0 is not fitted. Instead, it is defined as the inverse of critical over-density threshold : $b_0 = \frac{1}{\delta_c} = 0.593$. This value used in the Battaglia et al. model comes from an analytical study of the redshift of reionization on large scales (13). The new equation fitting for is, therefore:

$$b_{\rm mz}(k) = \frac{0.593}{(1 + k/k_0)^{\alpha}}. \qquad [11]$$

Figure 5 presents the posterior distributions for the best-fit parameters α and k_0. The corner plots indicate a Gaussian-like posterior distribution for both fitted parameters. The confidence regions, representing 68% of the posterior distribution and denoted by quartile lines, are narrow, indicating confidence in the obtained best-fit value. The rough look of the corner plot and the small number of bins is suspected to be due to the used python package for MCMC: *emcee*, having trouble parsing through small numbers. A potential solution would be to rescale the data by multiplying the whole array by a factor of 10.

Figure 6 presents the trace plots, showing the behaviour of the walkers throughout the iterations of the MCMC. The trace plot shows that the walkers general behaviour is horizontal, suggesting the walkers converged since traces plot showing a trend means convergence has not been reached. Moreover, the trace plot does not show are lost walkers, showing that the walkers have converged to similar high probability regions in their sampling. This behaviour indicates confidence in the fit.

Finally, Figure 7 takes a random selection of 100 parameter values in the chain to plot these to look at the fitting of the model with the data. The plotted best-fits are partially transparent, meaning that regions where the prediction is very tight, will show intense colours, while regions where the prediction is quite uncertain will show faint colours. The limited spread of the best-fit lines makes the different best-fits almost indistinguishable, meaning that there is a great confidence in the best-fit parameters. The data is in reasonable agreement with the model: the best-fit lines pass through 2/3 of the points and are replicating the shape.

Discussion

Results indicate that the algorithm successfully computes the linear bias with data 21cmFAST. Figure 3 shows a high concentration towards the center (low k values) for both fields and an exponential decay afterward. These observations are in

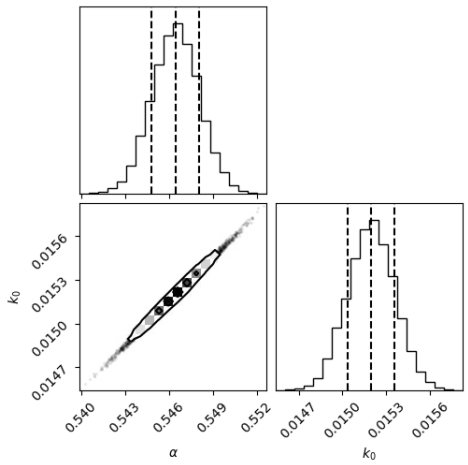

Fig. 5. Corner plots of the posterior distributions for the best-fit parameter α and β. The top-left plot shows the probability density distribution for the α, while the bottom-right plot shows the one for k_0. In both plots, the middle dotted line represents the mean value for the distribution, that can be attributed to the best fit value, while the first and last lines are quartiles, showing the region in which 68%, one σ, of the posterior distribution is, showing the upper and lower bounds of confidence in a similar way error bars would do. The bottom-right plots present the probability function of the two-dimensional parameter space, with darker zones representing higher probability regions for the best-fit parameters. All the plots are normalized.

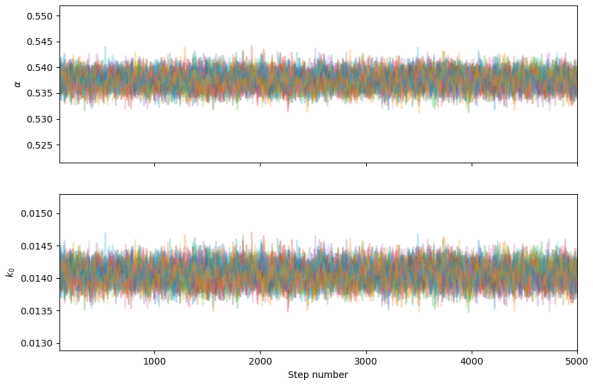

Fig. 6. Behaviour of the 32 walkers probing the probability regions of the parameter space of α (top plot) and k_0 (bottom plot). This shows the sampled values per walker throughout iterations.

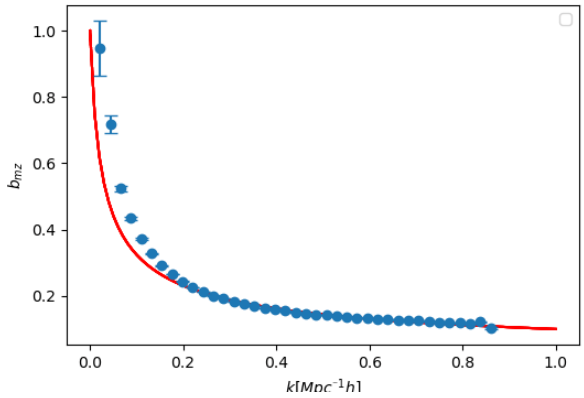

Fig. 7. Comparison between the linear bias data and a 100 best-fit α and k_0 parameters randomly selected in the parameter space.

concordance with the behaviour of the linear bias factor shown in Figure 4. Moreover, from a broad point of view, results show an agreement between the three-parameter function and the linear bias computed from 21cmFAST. The walker behaviour from Figure 6, the posterior distribution for the best-fit parameters, and the sample of best-fits show that the MCMC algorithm successfully sampled parameter space and reached convergence on the best-fit parameters, with great confidence. The best fits showed a reasonable fitting, especially for higher k. The three-parameter function and the linear bias computed from 21cmFAST. However, for the great confidence may be due to the low error bars, especially at high k. A potential source of error is the absence of systematic uncertainty in the data. Identifying the standard error as only the statistical uncertainty reduces the errors, especially at high k. This brings a level of confidence in the fit that can be non-representative of reality, while according to overweight of data points for the $k > 0.2$ range in the fitting. A possible solution to this overweighting would be modifying the k ranges averaged on to get more data points in the range $k < 0.2$, and less on the higher k. Another source of error in the algorithm is the assumed value for the b_0 parameter. Computing the value for the critical over-density with 21cmFAST's data will improve the algorithm's credibility.

The algorithm being functional, exploring the effect of the variation of 21cmFAST cosmological parameters on the bias parameters α and k_0. For example, modifying the ionization efficiency parameter that defines the ionization state and looking at the effect of this variation of the fiducial parameter would allow a better use of the Battaglia model.

Conclusion

This project aimed to construct an algorithm linking the free parameters of the linear bias in Battaglia et al. to the redshift of reionization field and the density field generated from 21cmFAST, and to verify the validity of the equation when applied to models containing no hydrodynamic simulations, like 21cmFAST.

Following the steps used by Battaglia et al. to parameterize their linear bias, the linear bias of 21cmFAST was computed. Slices of the magnitude square of the over-density at the mean redshift of reionization $\bar{z} = 7.22$, and the over-redshift of reionization, both in momentum space, were in agreement with the computed linear bias. Moreover, the walkers' behaviour f, the posterior distribution for the best-fit parameters, and the plotted sample of best-fits show that the MCMC algorithm successfully sampled parameter space and reached convergence on the best-fit parameters. The algorithm has its limitations and space for improvements, but results show that the project's goal is reached.

ACKNOWLEDGMENTS. I would like to thank my supervisor: prof. Adrian Liu, for his trust, his time, his precious guidance, and for giving me the opportunity of a first experience in cosmology research. I would also like to thank the whole cosmic dawn research group for their precious suggestions and for their warm welcome. Finally, I would like to thank my loving family and friends for their constant support.

References

1. N Battaglia, H Trac, R Cen, A Loeb, Reionization on Large Scales I: A Parametric Model Constructed from Radiation-Hydrodynamic Simulations. *The Astrophys. J.* **776**, 81 (2013) arXiv: 1211.2821.
2. M Tanabashi, et al., Review of Particle Physics. *Phys. Rev. D* **98**, 030001 (2018).
3. D Maoz, *Astrophysics in a Nutshell: Second Edition*. (Princeton University Press), (2016) Google-Books-ID: jfRlawEACAAJ.
4. S Furlanetto, SP Oh, F Briggs, Cosmology at Low Frequencies: The 21 cm Transition and the High-Redshift Universe. *Phys. Reports* **433**, 181–301 (2006) arXiv: astro-ph/0608032.
5. PA Carroll, et al., A high reliability survey of discrete Epoch of Reionization foreground sources in the MWA EoR0 field. *Mon. Notices Royal Astron. Soc.* **461**, 4151–4175 (2016).
6. H Trac, R Cen, A Loeb, Imprint of Inhomogeneous Hydrogen Reionization on the Temperature Distribution of the Intergalactic Medium. *The Astrophys. J.* **689**, L81 (2008) Publisher: IOP Publishing.
7. H Trac, UL Pen, A moving frame algorithm for high Mach number hydrodynamics. *New Astron.* **9**, 443–465 (2004) ADS Bibcode: 2004NewA....9..443T.
8. JP Paardekooper, CJH Kruip, V Icke, SimpleX2: radiative transfer on an unstructured, dynamic grid. *Astron. Astrophys.* **515**, A79 (2010).
9. JA Weber, AWA Pauldrach, JS Knogl, TL Hoffmann, Three-dimensional modeling of ionized gas - I. Did very massive stars of different metallicities drive the second cosmic reionization? *Astron. & Astrophys.* **555**, A35 (2013) Publisher: EDP Sciences.
10. A Mesinger, S Furlanetto, R Cen, 21cmfast: a fast, seminumerical simulation of the high-redshift 21-cm signal: 21cmfast. *Mon. Notices Royal Astron. Soc.* **411**, 955–972 (2011).
11. S Sharma, Markov Chain Monte Carlo Methods for Bayesian Data Analysis in Astronomy. *Annu. Rev. Astron. Astrophys.* **55**, 213–259 (2017) arXiv: 1706.01629.
12. S Giri, G Mellema, R Ghara, Optimal identification of HII regions during reionization in 21-cm observations. *Mon. Notices Royal Astron. Soc.* **479** (2018).
13. R Barkana, A Loeb, A Method for Separating the Physics from the Astrophysics of High-Redshift 21cm Fluctuations. *The Astrophys. J.* **624**, L65–L68 (2005) arXiv: astro-ph/0409572.